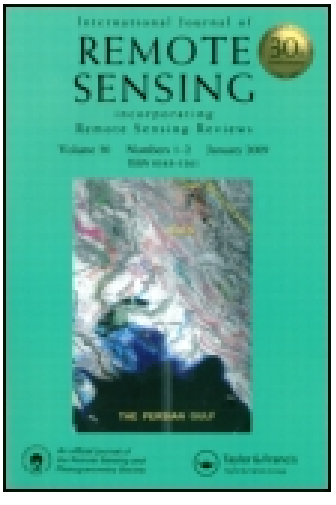

International Journal of Remote Sensing

Publication details, including instructions for authors and subscription information:
http://www.tandfonline.com/loi/tres20

ASTER ratio indices for supraglacial terrain mapping

A. K. Keshri [a] , A. Shukla [a] & R. P. Gupta [a]

[a] Department of Earth Sciences , Indian Institute of Technology Roorkee , Roorkee 247667, India

Published online: 26 Nov 2008.

To cite this article: A. K. Keshri , A. Shukla & R. P. Gupta (2009) ASTER ratio indices for supraglacial terrain mapping, International Journal of Remote Sensing, 30:2, 519-524, DOI: 10.1080/01431160802385459

To link to this article: http://dx.doi.org/10.1080/01431160802385459

International Journal of Remote Sensing
Vol. 30, No. 2, 20 January 2009, 519–524

Taylor & Francis
Taylor & Francis Group

Letter

ASTER ratio indices for supraglacial terrain mapping

A. K. KESHRI, A. SHUKLA and R. P. GUPTA*
Department of Earth Sciences, Indian Institute of Technology Roorkee, Roorkee 247667, India

(*Received 13 May 2008; in final form 1 August 2008*)

Supraglacial terrain, such as that found in the Himalayas, is typically composed of snow, ice, ice-mixed-debris (IMD) and debris. This letter presents a methodology for systematic discrimination and mapping of these supraglacial cover types using Advanced Spaceborne Thermal Emission and Reflection Radiometer (ASTER) data. The Normalized Difference Snow Index (NDSI) has been used previously for discrimination of snow/ice-bearing zones versus debris. Two new indices, the Normalized Difference Glacier Index (NDGI) and the Normalized Difference Snow Ice Index (NDSII), are presented. The combination of all three indices allows discrimination of snow, ice and IMD in a systematic manner.

1. Introduction

Supraglacial terrain is typically composed of four main cover types: snow, ice, ice-mixed-debris (IMD) and debris. (The term debris here is taken to include all rock materials lying on the glacier or adjacent to the glacier, as well as the adjoining valley rock.) Most previous studies have used the Normalized Difference Snow Index (NDSI) to discriminate snow/ice versus non-snow/ice regions. However, for more accurate mapping of glacial features, it is important to discriminate and map the spatial distribution of supraglacial cover types. To address this need, a systematic study of the spectral characteristics of supraglacial cover types was carried out using Advanced Spaceborne Thermal Emission and Reflection Radiometer (ASTER; Abrams and Hook 1998) data. Notable differences in the spectra of these cover types suggest that it should be possible to discriminate between them. For this purpose, two new ratio indices, the Normalized Difference Glacier Index (NDGI) and the Normalized Difference Snow Ice Index (NDSII), have been formulated using ASTER sensor data, which has been widely used in glaciological studies (Kargel *et al.* 2005). Discrimination of the supraglacial cover types is proposed using statistical thresholding of the normalized difference indices, and simple, sequential boolean logic.

2. Study area and data used

The Chenab basin in the Himalayas was selected as the test area for this study. An image of this region was acquired by ASTER on 8 September 2004. This date is during the post-monsoon season, and ensures the minimum coverage of temporary snow and maximum exposure of the glaciers. The data were preprocessed to Level-1B by the National Aeronautics and Space Administration (NASA).

*Corresponding author. Email: rpgupta.iitr@gmail.com

International Journal of Remote Sensing
ISSN 0143-1161 print/ISSN 1366-5901 online
http://www.tandf.co.uk/journals
DOI: 10.1080/01431160802385459

3. Methodology

3.1 *Image preprocessing*

The ASTER image was georeferenced using local topographic maps, 35 ground control points and a first-degree polynomial transformation, resulting in a root mean square (RMS) accuracy of 0.5 pixels. Orthocorrection of imagery is advisable in this rugged terrain; however, approximate georeferencing using image warping provided sufficient accuracy for this demonstration study.

The geometrically corrected image was radiometrically corrected by conversion of the digital number (DN) values to radiance using sensor calibration data, and then to at-satellite planetary reflectance using Markham and Barker's (1986) equation. The ASTER specific calibration parameters were obtained from Abrams and Hook (1998) and Thome *et al.* (1998). The conversion to reflectance is not strictly speaking necessary, but it does simplify interpretation of the results. Although anisotropic reflectance correction due to topography and bidirectional reflectance distribution function (BRDF) variations substantially improves spectral analysis in mountainous areas (Colby 1991, Sandmeier 1995), such corrections were not applied in this exploratory study. The demonstration study area is relatively limited, and the methods presented are relatively robust. However, for regional mapping over larger areas, such corrections would be essential.

3.2 *Computation of spectral indices*

3.2.1 Normalized Difference Snow Index (NDSI). The NDSI is defined as the difference of reflectance observed in a visible band (usually green) and the shortwave infrared (SWIR) band divided by the sum of the two reflectances. The index uses the spectral characteristics of snow/ice (figure 1): a high reflectance in the visible region and a strong absorption in the SWIR region (Dozier 1989, Hall *et al.* 1995).

The SWIR wavelength range of 1.55–1.70 μm typical in many current spaceborne multispectral sensors has usually been used for the computation of the NDSI. The

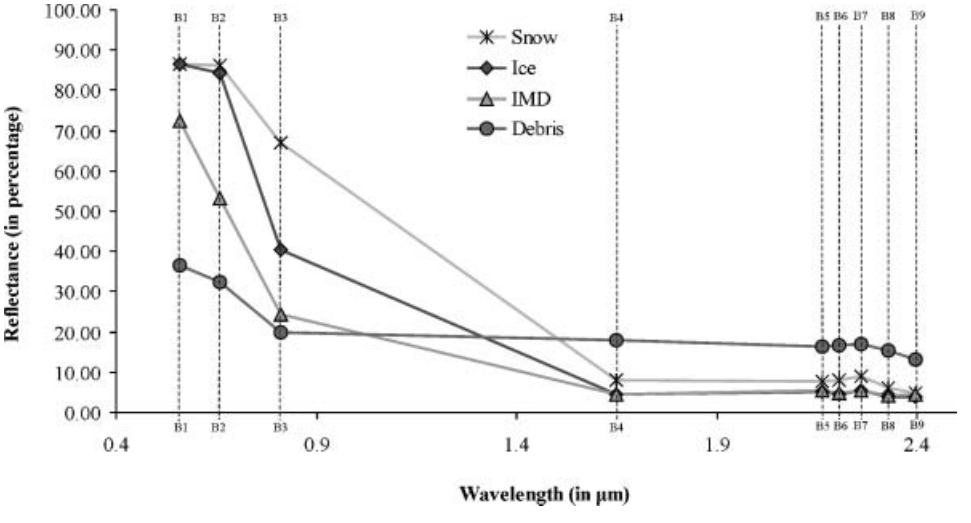

Figure 1. Spectral reflectance curves for snow, ice, ice-mixed-debris (IMD) and debris, as derived from ASTER data.

equivalent band at this wavelength for ASTER is B4, and hence this band has been used for the NDSI computation. Figure 2(*a*) shows that the NDSI frequency distribution for a test glacier in the study area is bimodal. The peak associated with low NDSI is associated with debris, and the peak associated with high NDSI is associated with the 'snow + ice + IMD' class.

Selection of an appropriate threshold value in the NDSI frequency distribution is a crucial task, as even a slight error may lead to overestimation or underestimation of the cover classes. Moreover, the thresholds may vary with different satellite sensors and also seasons (Dozier 1989, Hall *et al.* 1995). In this study a statistical approach of using the minimum value in the trough of the bimodal frequency distributions was adopted for selecting all thresholds (e.g. Gupta *et al.* 2005). For the NDSI frequency distribution for the study area, the observed threshold value of 0.61 appears to be slightly higher than the generally reported value (0.4; Dozier 1989, Hall *et al.* 1995), and may be attributed to the saturation of the ASTER B1 band over snow and possible seasonal variations in the spectral properties of the classes.

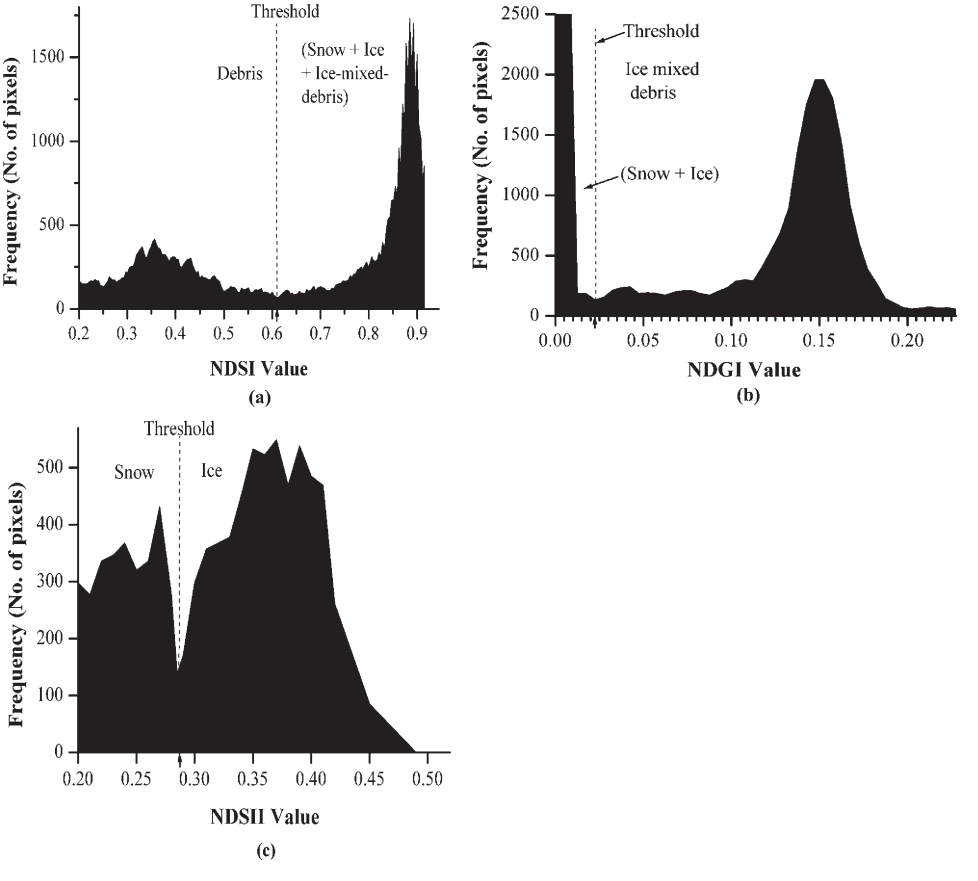

Figure 2. (*a*) NDSI frequency distribution showing bimodal character pertaining to 'snow + ice + IMD' versus debris. (*b*) NDGI frequency distribution showing bimodal character pertaining to snow/ice versus IMD. (*c*) NDSII frequency distribution showing bimodal character pertaining to snow versus ice.

3.2.2 Normalized Difference Glacier Index (NDGI). After the discrimination of 'snow + ice + IMD' surfaces from debris, the next step is to further discriminate within 'snow + ice + IMD' surfaces. For this purpose, the spectral characteristics of these supraglacial cover classes were studied in bands B1 and B2 (figure 1). It is clear that the spectral slope in these two bands for IMD is distinctly different from that of snow/ice, and thus the B1/B2 can potentially help to discriminate between these classes. Therefore, a new index, the NDGI, is proposed:

$$\mathrm{NDGI} = \frac{\mathrm{Green(B1)} - \mathrm{Red(B2)}}{\mathrm{Green(B1)} + \mathrm{Red(B2)}} \quad (1)$$

Figure 2(*b*) shows that the NDGI frequency distribution also possesses a bimodal distribution, and can be used for the discrimination of snow/ice versus IMD. The threshold value chosen for the study area data set was 0.025.

3.2.3 Normalized Difference Snow Ice Index (NDSII). The next step is the discrimination between snow and ice. An examination of the spectral slopes of snow and ice between bands B1 and B3 indicates the potential of this spectral region because the reflectance of ice declines towards the near infrared (NIR) band B3 (figure 1). Using the above characteristics, a second index, the NDSII, was formulated as:

$$\mathrm{NDSII} = \frac{\mathrm{Green(B1)} - \mathrm{NIR(B3)}}{\mathrm{Green(B1)} + \mathrm{NIR(B3)}} \quad (2)$$

Figure 2(*c*) shows the bimodal NDSII frequency distribution, representing snow and ice surfaces. The threshold value in the study area data set was found to be 0.28.

It is important to note that the threshold values for the two newly formulated indices are likely to be scene dependent, and an empirical analysis may be necessary for each case.

4. Results

4.1 *Mapping of debris, IMD, ice and snow*

A sequential classification using the previously defined NDSI and the two new indices, NDGI and NDSII, was used to map debris, IMD, ice and snow for the study (figure 3). The final classification map of the study area using this approach is shown in figure 4(*b*).

4.2 *Validation*

For the purpose of validating the classified output, a statistical error matrix-based approach was adopted (Congalton 1991). Due to the non-availability of any image data with spatial resolution higher than 15 m, the ASTER visible/near-infrared (VNIR) image was itself used as reference. The test sample constituting 50 pixels per class (a total of 200 pixels) was collected following the equalized random samplings scheme. Reference class values to each point were given on the basis of analysis of spectral curves and visual interpretation. The overall accuracy was 91%, with values of individual accuracies (user's and producer's accuracies) ranging from 87% up to 98% (table 1). Errors appear to be due to problems in discrimination between snow, ice, IMD and debris.

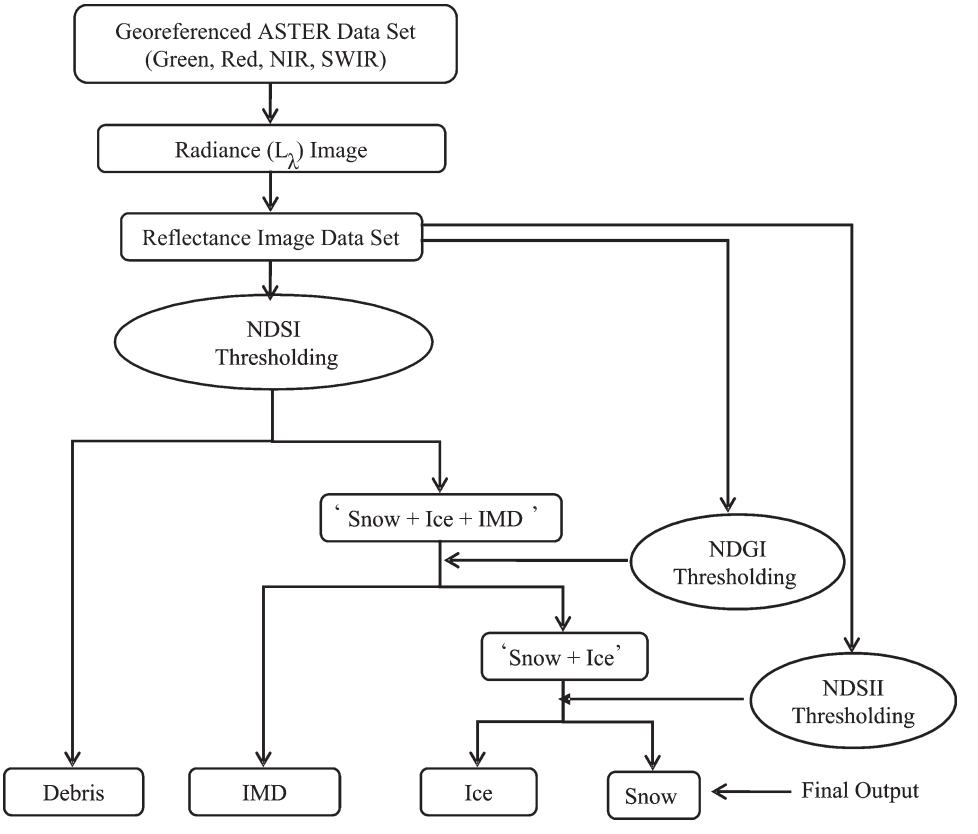

Figure 3. Conceptual flowchart for the sequential discrimination of debris, ice-mixed-debris (IMD), ice and snow using ASTER data.

5. Conclusions

Areal estimates of spatial distribution of various supraglacial cover types in glacial terrains are important for various glacier-related studies. In this letter, a simple yet effective methodology for systematic discrimination and mapping of various

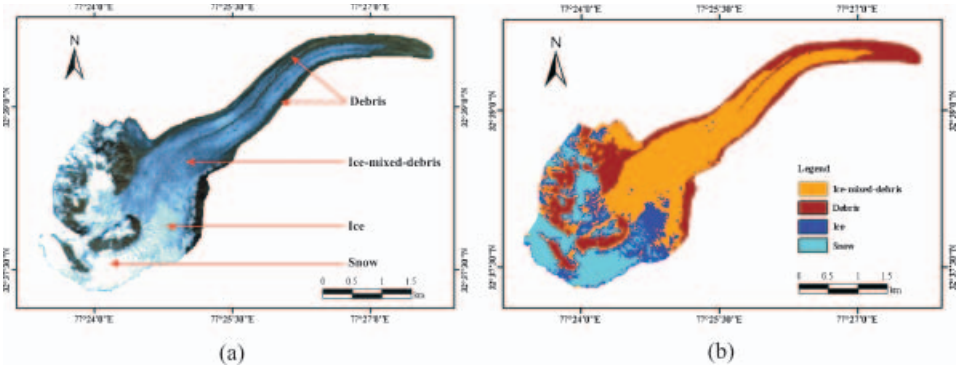

Figure 4. (*a*) A colour infrared composite of the test glacier. Note the various supraglacial cover types: snow, ice, ice-mixed-debris (IMD) and debris. (*b*) Classification map of the above glacier area.

Table 1. Error matrix for the supraglacial classification produced from ASTER data. Overall accuracy=91%.

	Reference data					
Classified	Snow	Ice	IMD	Debris	Total	User's accuracy (%)
Snow	46	4	0	0	50	92
Ice	1	44	5	0	50	88
IMD	0	0	45	5	50	90
Debris	0	1	2	47	50	94
Total	47	49	52	52	200	
Producer's accuracy (%)	98	90	87	90		

IMD, ice-mixed-debris.

supraglacial land-cover types, namely, snow, ice, IMD and debris, was developed using ASTER data. The differences in spectral slopes were used in formulating two new spectral indices, the NDGI and the NDSII. Using the NDSI, NDGI and NDSII, statistical thresholding and a boolean-logic approach, it is possible to sequentially discriminate and map debris, IMD, snow and ice.

Acknowledgements
We thank two unknown reviewers and Dr T. Warner for their constructive criticism.

References

Abrams, M. and Hook, S., 1998, *ASTER User Handbook, Version 1* (Pasadena: NASA/Jet Propulsion Laboratory).

Colby, D.J., 1991, Topographic normalization in rugged terrain. *Photogrammetric Engineering and Remote Sensing*, **57**, pp. 531–537.

Congalton, R.G., 1991, A review of assessing the accuracy of classifications of remotely sensed data. *Remote Sensing of Environment*, **37**, pp. 35–37.

Dozier, J., 1989, Spectral signature of alpine snow-cover from the Landsat Thematic Mapper. *Remote Sensing of Environment*, **28**, pp. 9–22.

Gupta, R.P., Haritashya, U.K. and Singh, P., 2005, Mapping dry/wet snow cover in the Indian Himalayas using IRS multispectral imagery. *Remote Sensing of Environment*, **97**, pp. 458–469.

Hall, D.K., Riggs, G.A. and Salomonson, V.V., 1995, Development of methods for mapping global snow-cover using moderate resolution spectroradiometer data. *Remote Sensing of Environment*, **54**, pp. 127–140.

Kargel, J.S., Abrams, M.J., Bishop, M.P., Bush, A., Hamilton, G., Jiskoot, H., Kääb, A., Kieffer, H.H., Lee, E.M. and Paul, F., 2005, Multispectral imaging contributions to global land ice measurements from space. *Remote Sensing of Environment*, **99**, pp. 187–219.

Markham, B.L. and Barker, J.L., 1986, Landsat MSS and TM post-calibration dynamic ranges, exoatmospheric reflectances and at-satellite temperatures. *EOSAT Landsat Technical Notes*, **1**, pp. 3–8.

Sandmeier, S., 1995, A physically-based radiometric correction model. Correction of atmospheric and illumination effects in optical satellite data of rugged terrain. PhD thesis. Remote Sensing Series, Vol. 26, Department of Geography, University of Zurich.

Thome, K., Palluconi, F., Takashima, T. and Masuda, K., 1998, Atmospheric correction for ASTER. *IEEE Transactions on Geosciences and Remote Sensing*, **36**, pp. 1199–1211.